Thermal Degradation Kinetics of Poly(imide-silica) Hybrid Films. I. Nanocomposites Prepared from HFPA and Bis(4-amino phenyl) Ether by Sol–Gel Process

M. Foroutan, S. Khoee

School of Chemistry, University College of Science, University of Tehran, Tehran, Iran

Received 13 May 2006; accepted 23 July 2006
DOI 10.1002/app.25898
Published online 8 March 2007 in Wiley InterScience (www.interscience.wiley.com).

ABSTRACT: Degradation kinetics of poly(imide-silica) hybrid films based on 4-4′-(hexafluro isopropylidene) bis(phthallic anhydride) and bis(4-aminophenyl) ether were investigated by thermogravimetric analysis TGA and DTG. The results indicated that the presence of inorganic content influence the mechanism of degradation of organic phase. Energy of activation of degradation for the hybrids with varying inorganic content was determined by the Flynn-Wall-Ozawa, pseudo first-order, van Krevelen methods. Although the values of E_a calculated by using various methods are different, there is a similar change trend of E_a between those methods. © 2007 Wiley Periodicals, Inc. J Appl Polym Sci 104: 3228–3235, 2007

Key words: thermal degradation kinetics; poly(imide-silica) hybrid films; nanocomposites; Flynn-Wall-Ozawa; pseudo first-order; van Krevelen

INTRODUCTION

Organic–inorganic composite materials are increasingly important because of their extraordinary properties not shared by conventional microcomposites counterparts, which arise from the synergism between properties of the components. These materials have gained much interest because of the remarkable changes in their properties such as electrical,[1] magnetic,[2] optical transparency,[3–5] mechanical, and thermal,[6–10] compared to pure organic polymers.

Since the inorganic phase is dispersed in the polymer matrix at a nanometric level, the organic–inorganic hybrid materials can be called nanocomposites (NC). NC can be obtained commonly by either sol–gel methods or intercalating a polymer, or a monomer followed by polymerization, into layered silicates. Recently, the degradation process organic–inorganic hybrid materials have been described by several kinetic models. Their results indicated that the presence of inorganic content influences the mechanism of degradation of organic phase.[11–13] Generally, kinetics analysis may effectively assist in probing degradation mechanism as well as in predicting the thermal stability of polymers.

Correspondence to: M. Foroutan (foroutan@khayam.ut.ac.ir).

Journal of Applied Polymer Science, Vol. 104, 3228–3235 (2007)
© 2007 Wiley Periodicals, Inc.

In this study, thermogravimetry (TG) and differential thermogravimetry (DTG) measurements of a novel system of poly(imide-silica) hybrid films with nanostructure (NC films) are reported and thermal degradation kinetics of films are studied by some kinds of calculating methods.

THEORETICAL BACKGROUND

There are several methods for calculating kinetics parameters that depend on the experimental conditions and the mathematical treatment of the data. The thermal degradation parameters were evaluated by two methods. The first method is nonisothermal different weight loss with constant heating rates to get average activation energy. Different heating rate of each conversion is the second method to measure activation energy.

Generally, the isothermal rate of conversion $d\alpha/dt$, which is dependent on the temperature, the mass change of the sample, can be expressed as:

$$\frac{d\alpha}{\mathrm{dt}} = K(T)f(\alpha) = A\exp\left(\frac{-E_a}{RT}\right)f(\alpha) \qquad (1)$$

where α is the degree of conversion, t is the time, $f(\alpha)$ is the function known as reaction model, $K(T)$ is the temperature-dependent rate constant according to Arrhenius equation, R is the gas constant, A is the pre-exponential factor, and E_a is the activation energy.

The integrated form of eq. (1) can be used for isothermal conditions as:

$$g(\alpha) = \int_0^{\alpha} \frac{d\alpha}{f(\alpha)} = K(T)t \tag{2}$$

In the case of polymer degradation, it is assumed that the rate of conversion is proportional to the concentration of material that has to react

$$f(\alpha) = (1-\alpha)^n \tag{3}$$

then

$$\frac{d\alpha}{dt} = A(1-\alpha)^n \exp(-E_a/RT) \tag{4}$$

The integrated form of eq. (1) with respect to temperature can be written as:

$$g(\alpha) = \int_0^{\alpha} \frac{d\alpha}{(1-\alpha)^n} \tag{5}$$

for $n = 1$:

$$g(\alpha) = \int_0^{\alpha} \frac{d\alpha}{(1-\alpha)^n} = -\ln(1-\alpha) \tag{6a}$$

for $n = 1$:

$$g(\alpha) = \int_0^{\alpha} \frac{d\alpha}{(1-\alpha)^n} = \frac{A}{\beta}\int_{T_0}^{T} \exp\left(\frac{-E}{RT}\right)dT \tag{6b}$$

Also, the dependence of the effective activation energy on the extent of conversion can be considered in kinetics analysis of degradation of polymers. There are isoconversional methods based on the assumption that the reaction model is independent of the heating program $T(t)$.[14,15] Because of complexity of thermal degradation of hybrid materials, flexible empirical nth order reaction model [eq. (4)], where n is empirical coefficient, has been chosen in some studies. The chosen models are fitted simultaneously to experimental datasets obtained at different heating rates.[16] The methods employed in this article are listed below.

Flynn-Wall-Ozawa method[17,18]

According to this method, for a set of nonisothermal TG experiments carried out at different constant heating rates β, the activation energy at any particular value of the conversion β is determined by the following equation:

$$\log\ \beta \cong 0.457\left(\frac{-E_a}{RT}\right) + \left[\log\left(\frac{AE_a}{R}\right) - \log g(\alpha) - 2.315\right] \tag{7}$$

where T is the absolute temperature, R is the gas constant, A is the pre-exponential factor, and $g(\alpha)$ is the conversion functional relationship. From the slope of the straight line, the activation energy, E_a obtained by plotting ln β vs. $1/T$.

Single-heating rate: Pseudo first-order method[19]

Pseudo first-order method uses the following equation:

$$\ln\left(\frac{-dW/dt}{W}\right) = E_a\left(\frac{-1}{RT}\right) + \ln A \tag{8}$$

where W, $-dW/dt$, and T are weight fraction remaining in TGA run, the rate of weight loss, and temperature, respectively. The plot of $\ln[(-dW/dt)/W]$ vs. $[-1/RT]$ will be a straight line with slope equal to the activation energy E_a.

van Krevelen method[20]

The van Krevelen equation, which is derived from eqs. (4) and (5) is:

$$\ln\left[\frac{1-(1-\alpha)^{1-n}}{1-n}\right] = \ln\left[\frac{A}{\beta}\left(\frac{0.368}{T_{\text{ref}}}\right)^{E/RT_{\text{ref}}}\left(\frac{E}{RT_{\text{ref}}}\right)^{-1}\right] + \left(\frac{E}{RT_{\text{ref}}} + 1\right)\ln T \tag{9}$$

The plot of $\ln[(1-(1-\alpha)^{1-n})/(1-n)]$ against $\ln T$ gives a straight line for a correctly chosen reaction order, and the values for E_a and A can be determined from the slope and intercept of the line, respectively.

EXPERIMENTAL

Materials

Tetraethoxysilane (TEOS) and bis(4-aminophenyl) ether were obtained from Merck Chemical 4,4′-(hexafluoroisopropylidene) bis(phthalic anhydride) (HFPA) was obtained from Hoescht-Celanese as electronic-grade material and used as received. Bis(4-aminophenyl) ether (ODA) was purified by sublimation before use. *N,N*-dimethylacetamide (DMAc) was dried over BaO, then distilled under reduced pressure, and stored at 0°C. Any other reagent was used without further purification.

Apparatus and procedure

Proton nuclear magnetic resonance (^{1}H NMR) spectra were recorded on a Bruker Avance 400 NMR spectrometer. Multiplicities of proton resonance are

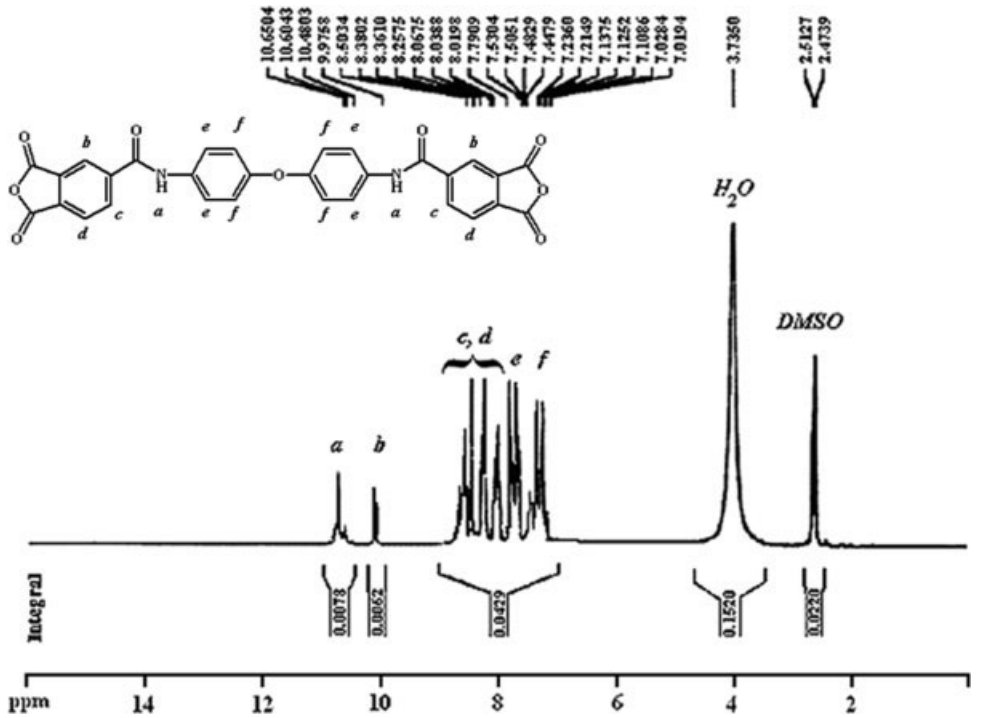

Figure 1 ^{1}H NMR spectrum of compound 3.

designated as singlet (s), doublet (d), triplet (t), quartet (q), multiplet (m), and broad (br). FTIR spectra were recorded on a Shimadzu FT/IR-4300 spectrophotometer from the films. Vibrational transition frequencies are reported in wave numbers (cm^{-1}). Band intensities are assigned as weak (w), medium (m), shoulder (sh), strong (s), and broad (br). Thermogravimetric analysis (TGA) were recorded on a Pyris 1 PerkinElmer under N_2 atmosphere with heating rate of 20°C/min and under O_2 atmosphere with heating rates of 10, 15, and 20°C/min. Scanning electron microscopy (SEM) was obtained from Cambridge S-360 SEM and ZEISS DSM 96A. Contact angles were measured by Krüss contact angle measuring system G10.

Sample preparation

Preparation of polyamic acid 3

At first, polyamic acid was prepared by adding 2.0 g (4.5×10^{-3} mol) HFPA 1 and 0.9 g (4.5×10^{-3} mol) bis(4-aminophenyl) ether 2 in 15-mL DMAc as the solvent into a round-bottomed flask equipped with a stirring magnet. The solution was stirred for 24 h at 0°C. The resulting viscous polyamic solution was poured into 120-mL methanol/water (1:1 v/v) solution. The precipitated polymer was filtered off and dried at 80°C for 10 h under vacuum to give 2.9 g (100% yield) amber-colored product as theprecursor in poly(imide-silica) synthesis.

FTIR: 3444 (s), 3049 (sh), 2937 (m, sh), 2484 (w), 1955 (w, br), 1784 (w, sh), 1731 (s), 1631 (s), 1545 (m), 1498 (s), 1402 (s), 1255 (s), 1211 (s), 1178 (s), 1070 (m), 1014 (m), 962 (m), 831 (m, sh), 719 (m, sh), 594 (m), 513 (w), 472 (w) cm^{-1}.

^{1}H NMR : (DMSO-d_6, TMS) : 7.077–7.096 (d, 1H), 7.670 (b, 1H), 7.736 (s, 1H), 7.867 (s, 1H), 7.928 (d,1H), 8.149 (d, 2H), 10.582 (s,2H).

Preparation of the poly(imide-silica) hybrid films

The desired amount of TEOS and 0.03 mL water were added to 0.3 g of 10% wt solution of polyamic acid in DMAc in a round-bottomed flask. The mixture was stirred for 6 h until the heterogeneous solution became homogeneous. The film was formed by casting the solution on a glass plate. After being dried at 60°C for 12 h, the resulting film was heated at 270°C for 3 h under N_2. Formation of poly(imide-silica) hybrid film was confirmed by means of FTIR spectroscopy.

Characterizations of poly(imide-silica) hybrid films

Chemical structure of the polyamic acid 3 was characterized by means of FTIR and ^{1}H NMR spectroscopy.

^{1}H NMR spectroscopy. The ^{1}H NMR spectrum of the compound 3 has been shown in Figure 1.

H_a and H_b are topologically nonequivalent and have different chemical shifts and they are affected

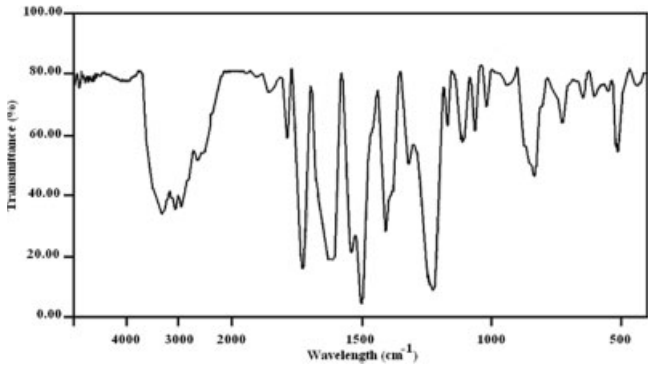

Figure 2 Typical FTIR spectra of poly(imide-silica) hybrid films.

by etheric oxygen and amidic nitrogen, respectively. Because of the conjugation of nitrogen electrons with carbonyl groups, the resonance effect on H_b is less than that of H_a and thus H_b is more deshielded than H_a. Therefore, H_a and H_b appear as a doublet at 7.08 and 7.21 ppm, respectively. The polyamic acid does not have any symmetric plane. So, H_c, $H_{c'}$, H_d, $H_{d'}$, H_e, and $H_{e'}$ have different chemical shifts. H_d and $H_{d'}$ are shielded more than the other protons because they are not affected by the anisotropy field of the carbonyl groups. These protons are split with c and c' protons with $J = 9$ Hz and also with e and e' protons with $J = 3$ Hz and they appear as a broad doublet peak in 7.40 and 7.47 ppm, respectively. H_c will appear as a broad peak in 7.67 ppm and $H_{e'}$ as a sharp peak in 7.87 ppm. Similarly, $H_{c'}$ appears at 7.92 and H_e at 8.14 ppm.

FTIR spectroscopy. Typical FTIR spectra of poly(imide-silica) hybrid films containing various amounts of silica have been shown in Figure 2. Disappearance of the strong acidic hydroxyl peak in NC1–NC10 confirms the formation of the desired polyimide. The conversion of polyamic acid to polyimide was proven by increasing the two overlapped imidic carbonyl intensities at 1728 (imide C=O asymmetric stretching) and 1784 cm^{-1} (imide C=O symmetric stretching). All of the spectra exhibited a strong absorbance at 1388 (C—N stretching) and 723 cm^{-1}, which shows the presence of the imidic heterocycle in these polymers. In addition, formation of silicon oxygen bonds was observed by two absorption bands at 1089 and 835 cm^{-1}. A narrow Si—O—Si vibration at 1089 cm^{-1} appeared in the hybrid NC2 indicating that the silicon environment in this hybrid film was more homogeneous and there are no SiO_4 clusters. However, this absorption band is broadened with increasing silica content for other hybrids. This reveals the occurrence of condensation reaction of the hydrolyzed TEOS to produce three-dimensional Si—O—Si network. The absorption bands in the range of 3116–3643 and 979 cm^{-1} are characterized as vibrational stretching of (Si—OH) and Si—O groups, respectively, that are formed during the hydrolysis of alkoxy groups in the presence of TEOS.

Poly(imide-silica) hybrid films containing 0 wt % silica (A). IR: 3641 (w), 3492 (m), 3116 (s, sh), 1784 (s),1720 (s, br), 1622 (m, sh), 1504 (s), 1436 (m,), 1382 (s, br), 1290 (s), 1259 (s, br), 1149 (s), 1110 (s, br), 1016 (m), 979 (s, sh), 881 (s), 835 (s), 721 (s), 638 (s), 601 (s, sh), 513 (s) cm^{-1}.

Poly(imide-silica) hybrid films containing 22 wt % silica (B). IR: 3562 (w), 3404 (m), 3114 (s, sh), 2929 (m), 2443 (m), 2083 (w), 1944 (m), 1888 (m), 1784 (s), 1745 (s, br), 1714 (s, br), 1623 (s, sh), 1436 (s), 1388 (s), 1365 (s), 1299 (s), 1234 (s, br), 1193 (s), 1147 (s, sh), 1114 (s), 1085 (s), 1016 (m), 979 (s, sh), 883 (s), 833 (s), 723 (s), 640 (m), 603 (s), 568 (m), 520 (s), 449 (s) cm^{-1}.

Poly(imide-silica) hybrid films containing 46 wt % silica (C). IR: 3645 (w), 3492 (m), 3116 (s, sh), 2929 (m), 2445 (m), 2083 (w), 1942 (m), 1890 (m), 1784 (s), 1741 (s, br), 1622 (s, sh), 1508 (s), 1436 (s), 1386 (s), 1298 (s), 1259 (s, br), 1195 (s), 1147 (s, sh), 1091 (s), 1016 (m), 979 (s, sh), 883 (s), 835 (s), 721 (s), 640 (m), 601 (s), 597 (m), 514 (m), 449 (s) cm^{-1}.

Poly(imide-silica) hybrid films containing 70 wt % silica (D). IR: 3643 (w), 3492 (m), 3114 (s, sh), 2962 (m), 2445 (m), 2083 (w), 1944 (m), 1888 (m), 1784 (s), 1708 (s, br), 1625 (s, sh), 1512 (s), 1438 (s), 1380 (s), 1298 (s), 1271 (s, br), 1207 (s, br), 1107 (s, br), 1016 (m), 979 (s, sh), 883 (s), 723 (s), 640 (m), 607 (s), 567 (m), 520 (m), 449 (s) cm^{-1}.

Scanning electron micrograph. Scanning electron micrographs of the fractured surface of the hybrid films are shown in Figure 3. They give important information about the morphology of the hybrid materials. For the system with a lower SiO_2 content, the phase heterogeneity is only slight and the polymer/SiO_2 interface is unclear [Fig. 3(a)]. When the TEOS percent is increased, the SiO_2 clusters are dispersed in polymer matrix with a clear phase separation [Fig. 3(b)].

Therefore, it is supposed that a nucleation/growth (NG) mechanism leads to this structure. The particle size is about 170 nm, the degree of heterogeneity is large, and the interface between these two phases is very sharp in these samples. The dispersed silica particles could be seen as white beads with the diameter of 110–230 nm and less than the wavelength of visible light (400–700 nm), which makes the hybrid films transparent or translucent. The particle size increases with increasing in silica content. The nanoscale of the particles is still retained in spite of increasing the TEOS content in the feed.

The contact angle of glass and NC5 hybrid film were determined to be 20° and 92°, respectively.

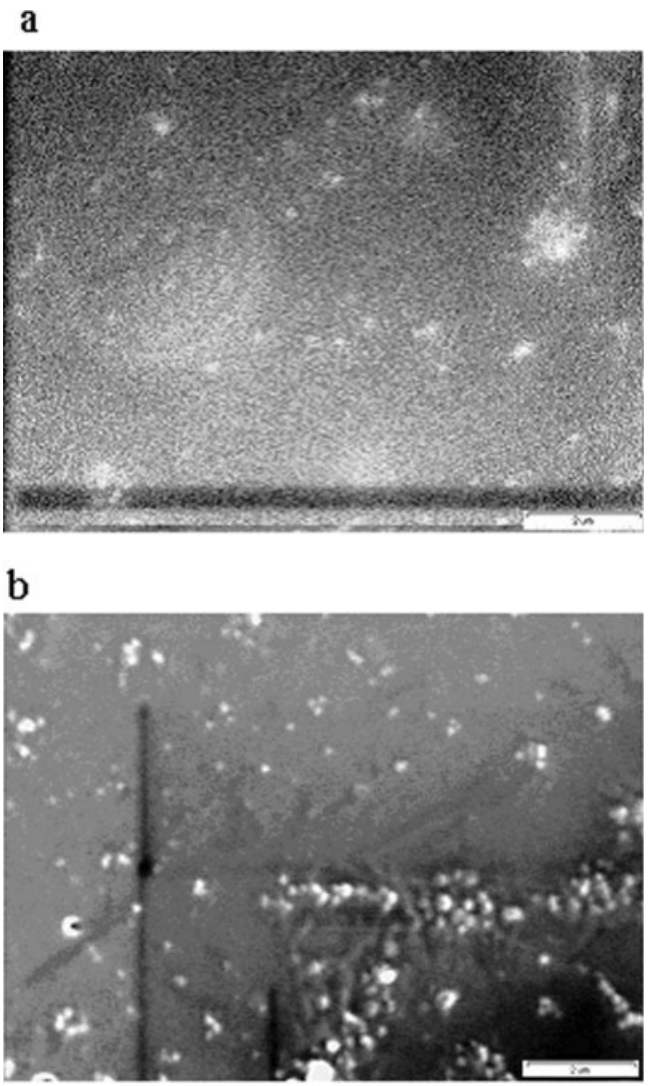

Figure 3 Scanning electron micrographs of the fractured surface of the hybrid films. (a) The polymer/SiO_2 interface is unclear and (b) the polymer matrix with a clear phase separation.

According to this result, the dispersity and adhesion of the films compared to glass were very low. So, water drops could diffuse very little on the surface of the hybrid films. This introduces a type of glass with wettability and a polarity of one-fourth relative to conventional glass.

RESULTS AND DISCUSSION

Generally, thermal degradation of NC films is complex, with more than one mechanism being operative depending on the degradation temperature and multiple peaks or asymmetric peaks with one or more shoulders can be seen in their thermograms.

Analysis of TG and DTG curves

The TG and DTG curves of NC films under nitrogen atmosphere are shown in Figure 4. As Figure 4(a) shows, the final weight residues at 846°C for A, B, C, and D samples are 47.5, 51.85, 51.98, and 51.03, respectively. It is found that the existence of the silica increases the weight residues of samples.

It may be seen from Figure 4(b) that polymer degrades by two main process corresponding to two peaks and a shoulder on the second peak. The degradation stages at 270–420 and 470–880 correspond to the decomposition of the aliphatic groups and imide-silica parts, respectively. As Figure 4(b) shows the DTG curves of all NC films at the first stage are same and the maximum rate temperature of weight loss at the first stage (T_{1m}) is independent of the silica component and is around 340°C. However, the maximum rate temperature of weight loss at the second stage (T_{2m}) varies with various values of silica content in the degradation. The maximum rate temperature of weight loss at the second stage (T_{2m}) of

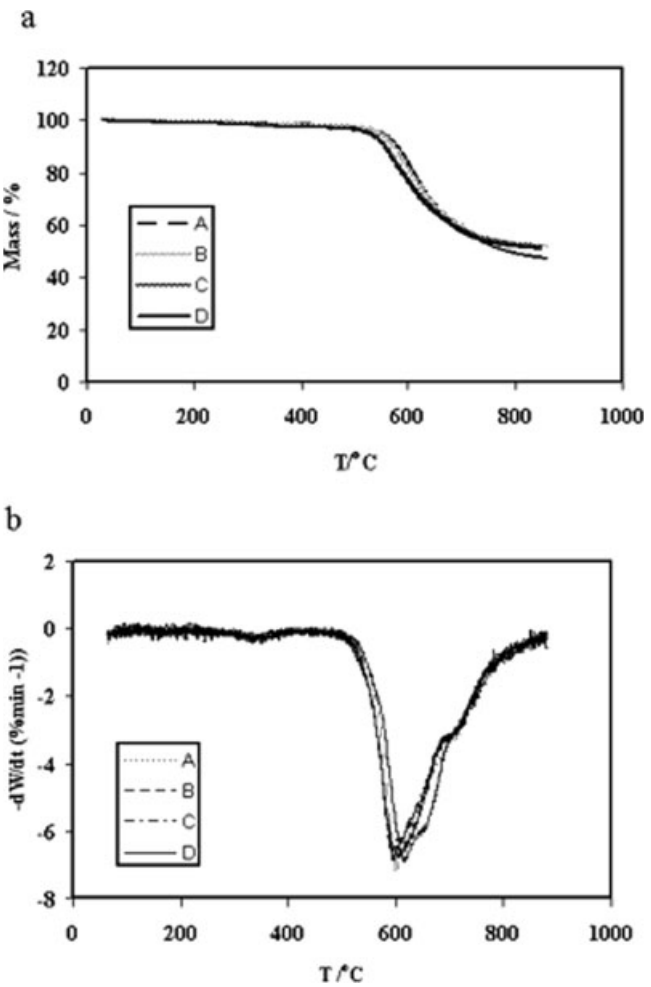

Figure 4 The TGA curves (a) and DTG curves (b) of NC films at heating rate 20°C/min for nitrogen.

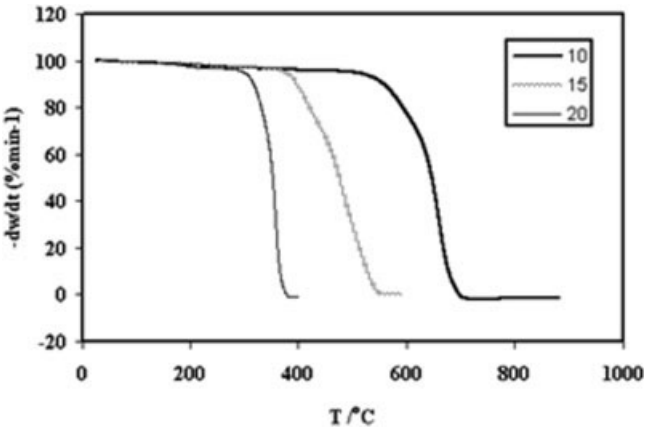

Figure 5 The TGA curves for the thermal decomposition of D film at heating rates 10, 15, and 20°C/min for nitrogen.

NC films A, B, C, and D are around 600°C. After degradation of silica parts of films B, C, and D at 600°C, they have similar behavior to sample A at shoulder on the second peak.

Figure 5 illustrates the TGA of film D at three heating rates of 10, 15, and 20°C/min. A high sensitivity of decomposition rate to heating rate can be seen for NC films. As shown in Figure 6, under air and oxygen, all NC films have degraded completely without leaving any noticeable residue, while under nitrogen, residual mass of film is equal to 47.15%.

Kinetic analysis

The TG curves of NC films obtained at heating rates of 10, 15, and 20°C/min are used as the basis for the determination of the apparent E_a as a function of conversion, using the Flynn-Wall-Ozawa method. By using eq. (7), the log β vs. $-1/RT$ plots from 5 to 90% conversion for the degradation of sample C are

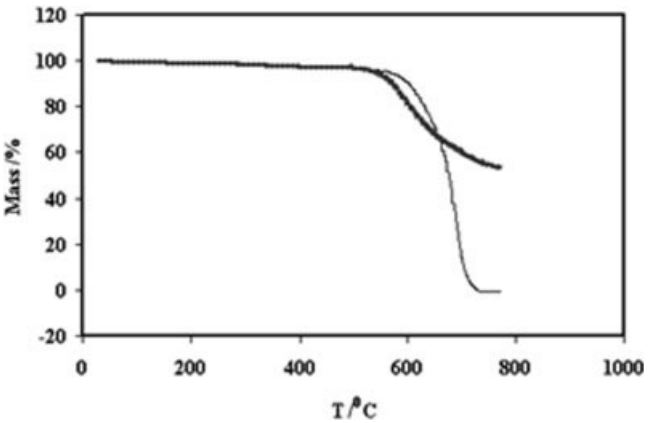

Figure 6 The TGA curves for the thermal decomposition of D film at heating rate 20°C/min for nitrogen (thick line) and oxygen and air (thin line).

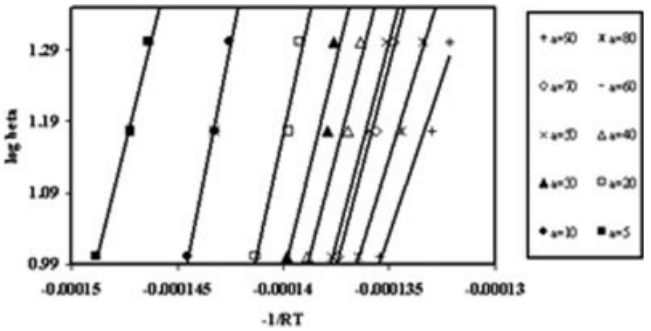

Figure 7 Flynn-Wall-Ozawa plots of C film at varying conversion for the first degradation stage.

shown in Figure 7. The resulting dependence of E_a on α for all NC films is shown in Figure 8. It can be seen that E_a of all films is not constant and the increase of activation energy with silica content is not linear. Also, there is no clear trend between the activation energy of degradation and the silica content of these films. The complexity of the reaction mechanism may be revealed in the form of a functional dependence of the apparent activation energy on the degree of conversion. It seems that film without silica (A) and hybrid films B, C, and D follow a different mechanism of degradation. The activation energy of hybrid films B, C, and D decreases with increasing silica content. The results suggest that silica may favor the degradation of films.

The reaction order of the nonisothermal degradation, n can be determined by the Kissinger method[21]:

$$n = 1.26\sqrt{s}$$

where s is the shape index of the differential thermal analysis curve for nonisothermal dynamic degradation. The shape index is defined as the absolute value of ratio of slopes of tangents to the DTG curve at the inflection point T_M. The reaction orders for degradation for NC films are shown in Table I. As

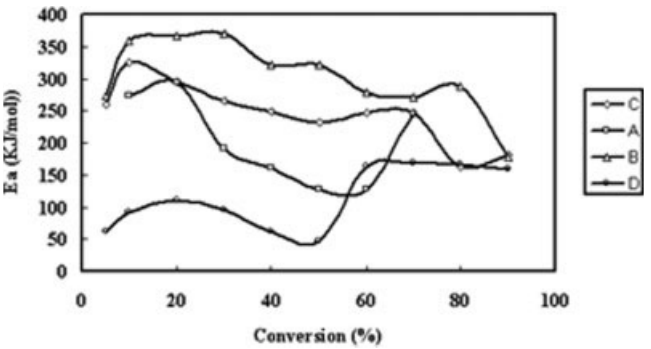

Figure 8 Activating energies calculated as a function of conversion for NC films using the Flynn-Wall-Ozawa method.

TABLE I
The Reaction Order of Thermal Degradation of NC Films for Nitrogen at 20°C/min

NC film	First peak	Second peak
A	1.37	2.19
B	1.34	2.78
C	1.38	2.13
D	1.33	2.97

Table I shows, the reaction order of thermal degradation of NC films at the first peak are close to one, and therefore it may be reasonable to calculate the activity energy of aliphatic groups of NC films by using pseudo first-order method. Figure 9 shows the plot of ln $[(-dW/dt)/W]$ vs. $-1/RT$ for heating rate of 20°C/min at nitrogen for film C. Activation energies of NC films A, B, C, and D have been obtained 72.520, 140.291, 54.742, and 51.554 kJ/mol, respectively.

A plot of $\left[\frac{1-(1-\alpha)^{1-n}}{1-n}\right]$ vs. ln T gives a straight line for a correctly chosen n (Fig. 10). This plot is possible to calculate the activation energies of degradation for aliphatic groups and silica-imide from the slopes. Table II summarizes the activation energies of NC films thermooxidative degradation. The order of decomposition reaction as determined by the Kissinger method has been used in calculating of activation energies for van Krevelen method.

In a similar work, poly(imide-silica) hybrid materials have been prepared by (3-aminopropyl) methyldiethoxysilane terminated amic acid, water, and tetramethoxysilane via a sol–gel process[13] and the apparent activation energy E_a of hybrids has been studied by the van Krevelen method. In these films, the value of E_a for siloxane segments decrease with increasing silica content, while those for imide segments increase. Also, in another research, thermal degradation kinetics of epoxy silica organic–inorganic hybrid, with 3-glycidyloxypropyl-trimethoxysilane

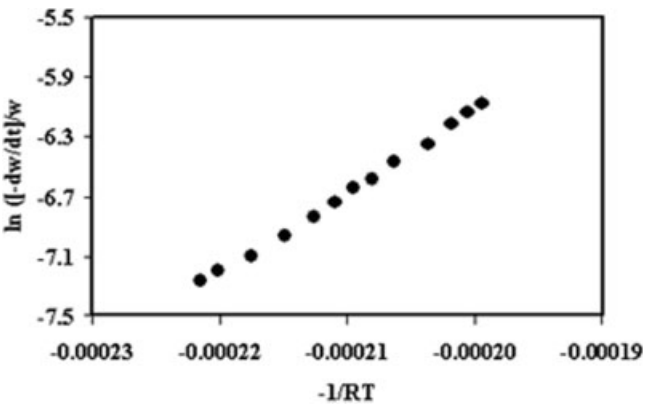

Figure 9 Pseudo first-order kinetics plot for NC films at heating rate 20°C/min for nitrogen.

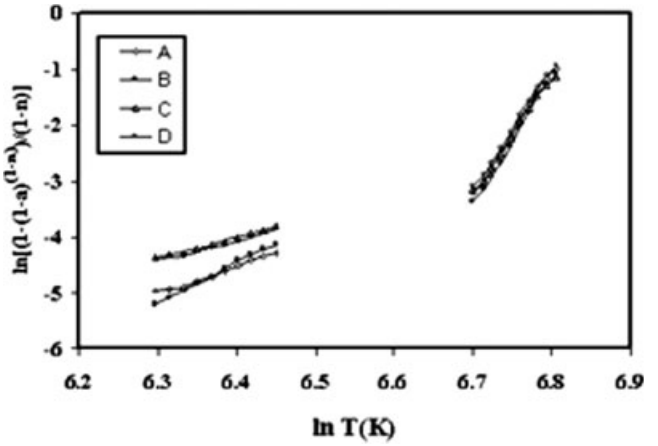

Figure 10 Plot of van Krevelen equation for degradation of NC films under nitrogen at 20°C/min.

have been studied[12] and it has been reported that hybrid materials have significantly higher E_a of degradation and follow a different mechanism of degradation than epoxy-amine system. As our results shown in Tables II, hybrid film B has the maximum activation energy between all hybrid films while film D has the maximum value of silica. It seems that hybrid films of the present work follow different behavior of degradation when compared with other hybrid films.

CONCLUSIONS

Degradation kinetic of organic–inorganic hybrid materials based on 4-4′-(hexafluro isopropylidene) bis(phthallic anhydride) and bis(4-aminophenyl) ether was investigated by TG and DTG thermograms. Several methods were used to determine the activation energies based on experiments conducted for the degradation of NC films at one heating rate under nitrogen atmosphere and at different heating rates under oxygen atmosphere. The kinetic parameters exhibit a dependence on heating rate and method of calculation. There is no correlation between the calculated values for activation energy and silica content in all methods, but there is a

TABLE II
Activation Energy (kJ/mol) for the Degradation of NC Films Calculated Using the van Krevelen and Friedman Methods for Nitrogen at 20°C/min

	van Krevelen	
NC film	First peak	Second peak
A	19.312	152.733
B	36.892	160.837
C	14.447	142.500
D	14.321	140.643

similar change trend of E_a between methods. When compared with other films, film D with lower silica content has lower activation energy and it is less heat stable than other films.

The authors thank Dr. A. R. Mahdavian, Iran Polymer and Petrochemical Institute, for useful comments.

References

1. Feller, J. F.; Linossier, I.; Levesque, G. Polym Adv Technol 2002, 13, 714.
2. Przybyl, A.; Wyslocki, J. J. J Mater Process Technol 2005, 19, 142.
3. Pignataro, B.; Pivin, J. C.; Marletta, G. Nucl Instrum Methods Phys Res B 2002, 191, 772.
4. He, R.; Qian, X. F.; Yin, J.; Bian, L. J.; Xi, H.; Zhu, Z. K. Mater Lett 2003, 57, 1351.
5. Chen, W. C.; Liu, W. C.; Wu, P. T.; Chen, P. F. Mater Chem Phys 2004, 83, 71.
6. Parija, S.; Nayak, S. K.; Verma, S. K.; Tripathy, S. S. Polym Compos 2004, 25, 646.
7. Choi, M. H.; Chung, L. J. J Appl Polym Sci 2003, 90, 2316.
8. Park, C. I.; Choi, W. M.; Kim, M. H.; Park, O. J Polym Sci Part B: Polym Phys 2004, 42, 1685.
9. Ellis, T. S.; D'Angelo, J. S. J Appl Polym Sci 2003, 90, 1639.
10. Kotsilkova, R. J Appl Polym Sci 2005, 97, 2499.
11. Sun, J. T.; Huang, T. D.; Gong, G. T.; Cao, H. L. Polym Degrad Stab 2006, 91, 339.
12. Macan, J.; Brnardic, I.; Orlic, S.; Ivankovic, H.; Ivankovic, M. Polym Degrad Stab 2006, 91, 122.
13. Wu, K. H.; Chang, T. C.; Wang, Y. T.; Chiu, Y. S. J Polym Sci Part A: Polym Chem 1999, 37, 2275.
14. Vyazovkin, S. J. Comput Chem 1997, 18, 393.
15. Vyazovkin, S. J. Comput Chem 2001, 22, 178.
16. Vyazovkin, S. J. Comput Chem 2006, 91, 122.
17. Flynn, J. H.; Wall, L. A. Polym Lett 1966, 4, 323.
18. Ozawa, T. J. Therm Anal 1970, 2, 301.
19. Chan, J. H.; Balke, S. T. Polym Degrad Stab 1997, 57, 135.
20. van Krevelen, D. W.; van Heerden, C.; Huntjen, F. J. Fuel 1951, 30, 253.
21. Kissinger, H. H. E. Anal Chem 1957, 29, 1702.